ELSEVIER

Inorganica Chimica Acta 223 (1994) 13–20

Inorganica Chimica Acta

Binuclear platinum(II) complexes of 1,1,4,7,10,10-hexaphenyl-1,4,7,10-tetraphosphadecane (P4) containing various bridging ligands as spacers between the P4 coordination units

Klaus Dillinger, Werner Oberhauser, Christian Bachmann, Peter Brüggeller*

Institut für Allgemeine, Anorganische und Theoretische Chemie, Universität Innsbruck, Innrain 52a, 6020 Innsbruck, Austria

Received by Editor 5 January 1994; received by Publisher 29 March 1994

Abstract

The former reported complex *cis,meso*-[Pt_2Cl_4P4] (**1**), where P4 is 1,1,4,7,10,10-hexaphenyl-1,4,7,10-tetraphosphadecane and which contains a chloro bridge only in solution, is fully characterized by an X-ray structure analysis: triclinic, $P\bar{1}$; $a=8.395(2)$, $b=11.675(2)$, $c=13.717(3)$ Å, $\alpha=92.54(3)$, $\beta=98.93(3)$, $\gamma=109.28(3)°$, $R=0.059$ for 2872 observed reflections ($F>6.0(F)$). It shows an open-mode dimer with a Pt–Pt distance of 6.916(1) Å and a *cis* P4 configuration. A comparison with the X-ray structure of *cis,rac*-[Pt_2Cl_4P4] (**2**) is given. **2** also contains a chloro bridge only in solution, and these chloro bridges of **1** or **2** are replaced by hydride in *rac*-[$Pt_2H_2(\mu\text{-H})P4](BF_4)$ (**3**), by pyridine in *rac*-[$Pt_2Cl_2(\mu\text{-}C_5H_5N)P4](BPh_4)_2$ (**4**), by pyrazolate (Pz) in *rac*-[$Pt_2Cl_2(\mu\text{-Pz})P4](BPh_4)$ (**5**), and by imidazolate (Im) in *meso*-[$Pt_2Cl_2(\mu\text{-Im})P4](BPh_4)$ (**6**) and *rac*-[$Pt_2Cl_2(\mu\text{-Im})P4](BPh_4)$ (**7**). In *rac*-[$Pt_2Cl_2(\mu\text{-Cl})(\mu\text{-dppa})P4](BPh_4)$ (**8**), where dppa is 1,2-bis(diphenylphosphino)acetylene, an additional dppa bridge occurs. The complexes have been characterized by $^{195}Pt\{^1H\}$, $^{31}P\{^1H\}$ and ^1H NMR spectroscopy, elemental analyses and melting points. **3**, **4**, **5**, **7** and **8** show that *rac*-P4 is flexible enough to allow the reaction with bridging ligands of very different sizes, whereas in the case of *meso*-P4 only the incorporation of imidazolate (**6**) is possible. This different behavior of *meso*- and *rac*-P4 is discussed with respect to the X-ray structures of **1** and **2**, showing that completely different rotation isomers could be responsible for the observed reactivity. In *meso*-[$Pt_2Cl(\mu\text{-Cl})(SnCl_3)P4](BPh_4)$ (**9**) the oxidative addition of $SnCl_2$ is only possible at a terminal Pt–Cl bond.

Keywords: Crystal structures; Platinum complexes; Polydentate phosphine ligand complexes; Binuclear complexes

1. Introduction

Recently, the preparation of *cis,meso*-[Pt_2Cl_4P4] (**1**), where P4 is 1,1,4,7,10,10-hexaphenyl-1,4,7,10-tetraphosphadecane, and *cis,rac*-[Pt_2Cl_4P4] (**2**) has been described [1a]. Interest in P4 containing dimers is due to the capacity of this ligand to produce unusual coordination modes [1b]. In this paper **1** is fully characterized by an X-ray structure analysis. Both **1** and **2** contain chloro bridges in solution (see Scheme 1) and are used as starting complexes for the reaction with various bridging ligands serving as spacers between the P4 coordination units. Thus, a variable metal–metal distance, which has earlier been stated to be important [2], is possible in these Pt(II) dimers.

The new complex *rac*-[$Pt_2H_2(\mu\text{-H})P4](BF_4)$ (**3**) (Scheme 1) contains the shortest bridge. The significance of Pt(II) hydrides has only recently been emphasized by some specific examples [3,4]. *Rac*-[$Pt_2Cl_2(\mu\text{-}C_5H_5N)P4](BPh_4)_2$ (**4**) and the pyrazolate (Pz) containing complex *rac*-[$Pt_2Cl_2(\mu\text{-Pz})P4](BPh_4)$ (**5**) also possess short bridges. Larger bridges like imidazolate (Im) occur in *meso*- and *rac*-[$Pt_2Cl_2(\mu\text{-Im})P4](BPh_4)$ (**6**,**7**). Interest in N-containing heterocycles as ligands stems from possible cytotoxicity [5] and magnetic and catalytic properties [6]. In the case of *rac*-[$Pt_2Cl_2(\mu\text{-Cl})(\mu\text{-dppa})P4](BPh_4)$ (**8**), where dppa is 1,2-bis(diphenylphosphino)acetylene, a very large bridge is used. Dppa is an interesting bridging ligand due to its different coordination modes [7]. Though the possibility of a bridging position has been described for the ligand

*Corresponding author.

SSDI 0020-1693(94)03979-X

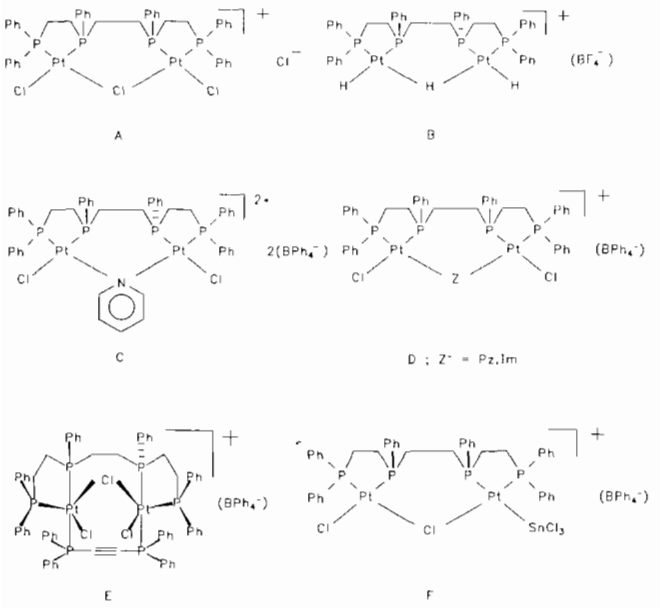

Scheme 1. Structure types observed in the dimers **1–9**. The P–Pt–P angles where the phosphorus atoms are connected by ethylene chains are constrained to about 85°. A: solution structure of *cis,meso*-$[Pt_2Cl_4P4]$ (**1**) and *cis,rac*-$[Pt_2Cl_4P4]$ (**2**); structure B occurs in *rac*-$[Pt_2H_2(\mu\text{-}H)P4](BF_4)$ (**3**), structure C in *rac*-$[Pt_2Cl_2(\mu\text{-}C_5H_5N)P4](BPh_4)_2$ (**4**), structure D in *rac*-$[Pt_2Cl_2(\mu\text{-}Pz)P4](BPh_4)$ (**5**) and in *meso*- and *rac*-$[Pt_2Cl_2(\mu\text{-}Im]P4](BPh_4)$ (**6**, **7**), structure E in *rac*-$[Pt_2Cl_2(\mu\text{-}Cl)(\mu\text{-}dppa)P4](BPh_4)$ (**8**), and structure F in *meso*-$[Pt_2Cl(\mu\text{-}Cl)(SnCl_3)P4](BPh_4)$ (**9**).

$SnCl_2$ [8], the oxidative addition of $SnCl_2$ occurs at a terminal Pt–Cl bond in *meso*-$[Pt_2Cl(\mu\text{-}Cl)(SnCl_3)P4](BPh_4)$ (**9**).

In the cases of **3**, **4**, **5** and **8** the reaction with the corresponding bridging ligands has only been possible for the *rac*-diastereomers. These different reactivities of **1** and **2** are discussed in view of their X-ray structures.

2. Experimental

2.1. Reagents and chemicals

Reagent grade chemicals were used as received unless stated otherwise. 1,1,4,7,10,10-Hexaphenyl-1,4,7,10-tetraphosphadecane (P4) and 1,2-bis(diphenylphosphino)acetylene (dppa) were purchased from Strem Chemical Co. $Na(BPh_4)$ was of purissimum grade quality and was received from Merck-Schuchardt. $Na(BH_4)$, $Na(BF_4)$, anhydrous $SnCl_2$, N-containing heterocycles and all organic solvents were obtained from Fluka. Solvents used for NMR measurements and crystallization purposes were of purissimum grade quality. $Na_2PtCl_4 \cdot 4H_2O$ was received from Fluka.

2.2. Instrumentation

Fourier-mode $^{195}Pt\{^1H\}$, $^{31}P\{^1H\}$ and ^1H NMR spectra were obtained by use of a Bruker AC-200 spectrometer (internal deuterium lock) and were recorded at 43.02, 80.96 and 200 MHz, respectively. Positive chemical shifts are downfield from the standards, where 1.0 M Na_2PtCl_6, 85% H_3PO_4 and TMS were used as standards, respectively.

2.3. X-ray data collection

The X-ray data collection was performed on a Siemens P4 diffractometer. Colorless crystals of *cis,meso*-$[Pt_2Cl_4P4]$ (**1**) were sealed into a capillary. The lattice was found to be triclinic by standard procedures using the software of the Siemens P4 diffractometer. No decay in the intensities of three standard reflections was observed during the course of data collection. The data were corrected for Lorentz and polarization effects. The empirical absorption correction was based on ψ-scans of nine reflections ($\theta = 75$–$105°$, $\chi = 10$–$350°$) [9].

2.4. Solution and refinement of the structure

All structure determination calculations were done on a 80486-PC using the PC-version of SHELXTL PLUS [10]. The position of the platinum atom was found by the Patterson method. Other atom positions were located from successive difference Fourier maps. Two molecules of methylene chloride per unit cell were included in the isotropic refinement. Two phenyl rings were anisotropically refined, one phenyl ring as a group. Final refinement was carried out with anisotropic thermal parameters for all other non-hydrogen atoms except for methyl chloride. Hydrogen atoms were included using a riding model with fixed isotropic U. The final R value of 0.059 was computed for 205 parameters and 2872 reflections. Upon convergence (shifts $< 0.13\sigma$) the last Fourier difference map showed no significant features. The structure determination is summarized in Table 1. Table 2 shows positional parameters for *cis,meso*-$[Pt_2Cl_4P4]$ (**1**).

2.5. Separation of the stereoisomers of P4

Commercial P4 was separated by fractional crystallization to give the pure *meso*- and *rac*-diastereomer, respectively, according to Brown and Canning [11].

2.6. Syntheses of Pt(II) complexes

A Schlenk apparatus and oxygen-free, dry Ar were used in the syntheses of all complexes. Solvents were degassed by several freeze–pump–thaw cycles prior to use. *Cis,meso*-$[Pt_2Cl_4P4]$ (**1**), *cis,rac*-$[Pt_2Cl_4P4]$ (**2**) and *rac*-$[Pt_2Cl_2(\mu\text{-}Cl)P4](BF_4)$ were prepared as described earlier [1a]. *Cis,meso*-$[Pt_2Cl_2(\mu\text{-}Cl)P4](BPh_4)$ and *cis,rac*-$[Pt_2Cl_2(\mu\text{-}Cl)P4](BPh_4]$ were prepared via metathesis of **1** or **2** with $Na(BPh_4)$.

Table 1
Structure determination summary for *cis,meso*-[Pt_2Cl_4P4] (**1**)

Formula	$C_{42}H_{42}Cl_4P_4Pt_2 \cdot 2CH_2Cl_2$
Formula weight	1372.4
Color; habit	colorless; irregular
Crystal system	triclinic
Space group	$P\bar{1}$
a (Å)	8.395(2)
b (Å)	11.675(2)
c (Å)	13.717(3)
α (°)	92.54(3)
β (°)	98.93(3)
γ (°)	109.28(3)
V (Å^3)	1247.0
T (K)	293
Z	1
Crystal dimensions (mm)	0.15×0.2×0.3
D_{calc} (Mg/m^3)	1.828
Radiation (Å)	Mo Kα (λ=0.71073)
μ (mm^{-1})	6.191
F(000)	1324
Range of transmission factors	0.30–0.62
Diffractometer	Siemens P4
Monochromator	highly oriented graphite crystal
Scan type	2θ-θ
Scan speed (°/min)	variable; 2.00 to 29.30 in ω
2θ Range (°)	7.0–45.0
Index ranges	$-1<h<11$, $-16<k<15$, $-19<l<19$
Reflections collected	8632
Independent reflections	7263 (R_{int}=0.037)
Observed reflections	2872 ($F>6.0\sigma(F)$)
No. parameters refined	205
Final R indices (observed data)	
R	0.059
R_w[a]	0.064
Goodness-of-fit	1.28
Largest and mean Δ/σ	0.128, 0.003
Largest difference peak (e Å^{-3})	2.00
Largest difference hole (e Å^{-3})	−1.32

[a] $w^{-1}=\sigma^2(F)+0.00050F^2$.

Table 2
Atomic coordinates (×10^4) and equivalent isotropic displacement coefficients (Å^2×10^3)

	x	y	z	U_{eq}[a]
Pt(1)	550(1)	2968(1)	3283(1)	28(1)
Cl(1)	2262(6)	2851(4)	2084(3)	49(2)
Cl(2)	2991(7)	3583(5)	4551(4)	59(2)
P(1)	−1764(6)	2511(4)	2119(3)	36(2)
P(2)	−1116(7)	3053(4)	4369(3)	40(2)
Cl(5)	3411(11)	3905(7)	7497(6)	115(2)
Cl(6)	5859(16)	2795(11)	7149(9)	192(5)
C(1)	−3645(24)	2197(17)	2713(14)	56(8)
C(2)	−3212(25)	3029(18)	3671(14)	57(9)
C(3)	−272(28)	4394(13)	5287(12)	56(9)
C(11)	−2155(23)	1153(17)	1240(12)	48(8)
C(12)	−2060(29)	1276(22)	281(16)	75(12)
C(13)	−2095(34)	261(25)	−330(20)	104(15)
C(14)	−2605(33)	−867(23)	10(19)	86(13)
C(15)	−2663(45)	−953(24)	966(21)	131(19)
C(16)	−2510(33)	42(16)	1570(16)	81(11)
C(21)	−1770(24)	3781(16)	1418(13)	45(8)
C(22)	−444(25)	4872(14)	1617(12)	46(8)
C(23)	−453(29)	5828(21)	1047(17)	76(11)
C(24)	−1803(39)	5662(31)	288(17)	97(17)
C(25)	−3122(35)	4617(26)	64(17)	83(14)
C(26)	−3150(30)	3638(23)	637(14)	77(11)
C(31)	−1571(27)	1778(17)	5123(12)	44(4)
C(32)	−2715	641	4692	549(64)
C(33)	−3039	−358	5246	529(62)
C(34)	−2218	−220	6231	85(7)
C(35)	−1074	916	6662	204(19)
C(36)	−750	1916	6108	236(21)
C(7)	5217(33)	4021(23)	7007(19)	99(8)

[a] For anisotropic atoms, the U value is U_{eq}, calculated as $U_{eq}=\frac{1}{3}\Sigma_i\Sigma_j U_{ij}a^*_i a^*_j A_{ij}$ where A_{ij} is the dot product of the ith and jth direct space unit cell vectors.

2.6.1. *Rac*-[$Pt_2H_2(\mu$-H)P4](BF$_4$) (3)

Rac-[$Pt_2Cl_2(\mu$-Cl)P4](BF$_4$) (0.2 mmol, 0.250 g) was suspended in 2.5 ml of absolute EtOH at room temperature. Under stirring, $NaBH_4$ (0.6 mmol, 0.024 g) was added in small portions. The slurry was stirred for 24 h, and its color turned to yellow. 5 ml of H_2O were added to the suspension. The yellow precipitate was filtered off, washed several times with H_2O and 1:2 EtOH/H_2O, and dried in vacuo: yield 0.173 g (75%); m.p. > 300 °C dec. *Anal.* Calc. for $C_{42}H_{45}BF_4P4Pt_2$: C, 43.8; H, 3.9. Found: C, 43.5; H, 3.8%.

2.6.2. *Rac*-[$Pt_2Cl_2(\mu$-C_5H_5N)P4](BPh$_4$)$_2$ (4)

Cis,rac-[Pt_2Cl_4P4] (**2**) (0.1 mmol, 0.120 g) and Na(BPh$_4$) (0.2 mmol, 0.068 g) were suspended in 12 ml dry CH_2Cl_2 at room temperature. Under stirring, pyridine (0.1 mmol, 0.0079 g) was added dropwise via a syringe. The slurry was stirred at 37 °C for 20 h. The color of the suspension turned from yellowish-white to brown. 10 ml of n-hexane was added to the slurry and the brown precipitate was filtered off, washed several times with H_2O and dried in vacuo. The brown powder was recrystallized from CH_2Cl_2/n-hexane: yield 0.129 g (70%); m.p. = 186 °C dec. *Anal.* Calc. for $C_{95}H_{87}B_2Cl_2NP4Pt_2$: C, 61.7; H, 4.7; N, 0.8. Found: C, 61.5; H, 4.6; N, 0.7%.

2.6.3. *Rac*-[$Pt_2Cl_2(\mu$-Pz)P4](BPh$_4$) (5)

Cis,rac-[Pt_2Cl_4P4] (**2**) (0.1 mmol, 0.120 g), pyrazole (0.1 mmol, 0.007 g), NaOH (0.1 mmol, 0.004 g) and Na(BPh$_4$) (0.1 mmol, 0.034 g) were suspended in CH_2Cl_2/MeOH (1:1). The slurry was stirred at 33 °C for 20 h. The color of the solution turned yellow. The solvent was completely evaporated and 10 ml of H_2O were added. The suspension was filtered and the precipitate washed several times with H_2O and dried in vacuo. The pale brown powder was recrystallized from CH_2Cl_2/n-hexane: yield 0.099 g (65%); m.p. > 250 °C dec. *Anal.* Calc. for $C_{69}H_{65}BCl_2N_2P4Pt_2$: C, 54.6; H, 4.3; N, 1.9. Found: C, 54.3; H, 4.3; N, 2.1%.

2.6.4. Meso-[$Pt_2Cl_2(\mu$-Im)P4](BPh$_4$) (6)

Cis,meso-[$Pt_2Cl_2(\mu$-Cl)P4](BPh$_4$) (0.1 mmol, 0.149 g), imidazole (0.1 mmol, 0.007 g) and NaOH (0.1 mmol, 0.004 g) were suspended in 12 ml CH_2Cl_2/MeOH (1:1). The slurry was stirred at room temperature for 20 h. The brown color of the solution intensified. The solvent was completely evaporated and 10 ml of H_2O were added. The suspension was filtered, the precipitate washed several times with H_2O and dried in vacuo. The brown powder was recrystallized from CH_2Cl_2/n-hexane: yield 0.106 g (70%); m.p. = 199 °C dec. *Anal.* Calc. for $C_{69}H_{65}BCl_2N_2P4Pt_2$: C, 54.6; H, 4.3; N, 1.9. Found: C, 54.8; H, 4.5; N, 2.2%.

2.6.5. Rac-[$Pt_2Cl_2(\mu$-Im)P4](BPh$_4$) (7)

This complex was prepared in an analogous manner to **6** except that DMF/MeOH (1:1) was used and the slurry was stirred at 80 °C for 24 h: yield 0.096 g (63%); m.p. = 195 °C dec. *Anal.* Calc. for $C_{69}H_{65}BCl_2N_2P4Pt_2$: C, 54.6; H, 4.3; N, 1.9. Found: C, 54.7; H, 4.4; N, 2.1%.

2.6.6. Rac-[$Pt_2Cl_2(\mu$-Cl)(μ-dppa)P4](BPh$_4$) (8)

Cis,rac-[Pt_2Cl_4P4] (**2**) (0.1 mmol, 0.120 g), dppa (0.1 mmol, 0.039 g) and Na(BPh$_4$) (0.1 mmol, 0.034 g) were suspended in 5 ml CH_2Cl_2. The slurry was stirred at 33 °C for 35 h. The solvent was completely evaporated and 10 ml of H_2O were added. The suspension was filtered and the precipitate washed several times with H_2O and dried in vacuo. The white powder was recrystallized from CH_2Cl_2/n-hexane: yield 0.160 g (85%); m.p. = 150 °C dec. *Anal.* Calc. for $C_{92}H_{82}BCl_3P_6Pt_2$: C, 58.7; H, 4.4. Found: C, 58.7; H, 4.3%.

2.6.7. Meso-[$Pt_2Cl(\mu$-Cl)($SnCl_3$)P4](BPh$_4$) (9)

Cis,meso-[$Pt_2Cl_2(\mu$-Cl)P4](BPh$_4$) (0.1 mmol, 0.149 g) and anhydrous $SnCl_2$ (0.11 mmol, 0.021 g) were suspended in 10 ml dry CH_2Cl_2. The slurry was stirred at 37 °C for 42 h. The color of the solution turned yellow. 10 ml of dry CH_2Cl_2 were added and the solution was filtered. After addition of 20 ml n-pentane a yellow powder was obtained. It was recrystallized from CH_2Cl_2/n-pentane: yield 0.126 g (75%); m.p. = 225 °C dec. *Anal.* Calc. for $C_{66}H_{62}BCl_5P4SnPt_2$: C, 47.3; H, 3.7. Found: C, 47.1; H, 3.8%.

3. Results

In order to characterize *cis,meso*-[Pt_2Cl_4P4] (**1**) definitely and to make a comparison with the structure of *cis,rac*-[Pt_2Cl_4P4] (**2**) [1a] possible, the solid state structure of **1** was determined by X-ray crystallography. A view of **1** is given in Fig. 1. Table 3 contains selected bond distances and bond angles.

The crystal structure of **1** consists of discrete *cis,meso*-[Pt_2Cl_4P4] molecules and two molecules of CH_2Cl_2 per unit cell. The presence of these solvent molecules is the reason for the rapid decomposition of the crystals in air due to desolvation. *Cis,meso*-[Pt_2Cl_4P4] is located on a center of symmetry. The square-planar coordinations of the platinum atoms are slightly distorted. Similar to *cis,rac*-[Pt_2Cl_4P4] (**2**) this is mainly a consequence of the two chelate five-rings constraining the P–Pt–P angles to 87.1(2)°. This leads to an opening of the P–Pt–Cl angles to 91.2(2) and 91.0(2)°, respectively, and to smaller than ideal *trans* angles of 176.1(2) and 178.3(2)°. However, the Pt–Cl and Pt–P bond distances remain identical within the standard deviations. In contrast to **2** the chloride and phosphorus ligands surrounding a platinum atom deviate from a plane through Cl1, Cl2, P1 and P2 in **1** (Cl1: −0.034, Cl2: 0.035, P1: 0.038, P2: −0.038 Å). The platinum atom deviates −0.029 Å from this plane towards the phenyl ring of the PPh group. The Pt–Pt distance of 6.916(1) Å is longer than in **2** (6.338(1) Å).

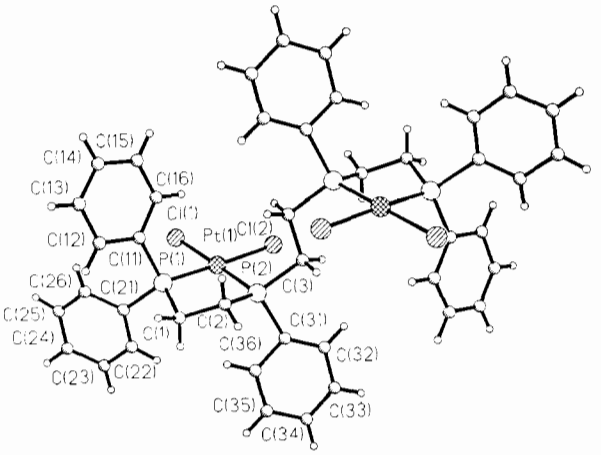

Fig. 1. View of *cis,meso*-[Pt_2Cl_4P4] (**1**), showing the atomic numbering.

Table 3
Selected bond distances (Å) and bond angles (°) for *cis,meso*-[Pt_2Cl_4P4] (**1**)

Pt(1)–Cl(1)	2.374(5)	Pt(1)–Cl(2)	2.356(5)
Pt(1)–P(1)	2.211(4)	Pt(1)–P(2)	2.215(6)
P(1)–C(1)	1.827(22)	P(1)–C(11)	1.854(19)
P(1)–C(21)	1.804(19)	P(2)–C(2)	1.859(22)
P(2)–C(3)	1.831(15)	P(2)–C(31)	1.821(19)
C(1)–C(2)	1.518(27)	C(3)–C(3A)	1.617(31)
Cl(1)–Pt(1)–Cl(2)	90.7(2)	Cl(1)–Pt(1)–P(1)	91.2(2)
Cl(2)–Pt(1)–P(1)	176.1(2)	Cl(1)–Pt(1)–P(2)	178.3(2)
Cl(2)–Pt(1)–P(2)	91.0(2)	P(1)–Pt(1)–P(2)	87.1(2)
Pt(1)–P(1)–C(1)	108.7(6)	Pt(1)–P(1)–C(11)	115.2(7)
C(1)–P(1)–C(11)	106.6(8)	Pt(1)–P(1)–C(21)	112.0(5)
C(1)–P(1)–C(21)	105.0(10)	C(11)–P(1)–C(21)	108.7(8)
Pt(1)–P(2)–C(2)	108.1(7)	Pt(1)–P(2)–C(3)	115.4(7)
C(2)–P(2)–C(3)	108.2(10)	Pt(1)–P(2)–C(31)	114.3(8)
C(2)–P(2)–C(31)	106.9(9)	C(3)–P(2)–C(31)	103.5(8)
P(1)–C(1)–C(2)	110.1(12)	P(2)–C(2)–C(1)	108.6(16)
P(2)–C(3)–C(3A)	108.8(14)		

However, the most striking feature is the appearance of two completely different rotation isomers in the solid state structures of **1** and **2**. This is shown in Fig. 2, where views perpendicular to the central P(2)- - -(P2a) vector are given for **1** and **2**, respectively. The two coordination units each containing a platinum, two phosphorus and two chlorine atoms are rotated towards completely different directions in **1** and towards approximately the same direction in **2**. To account for these different orientations the M- - -P_{int}- - -P'_{int}- - -M′ torsional angles, where P_{int} and P'_{int} are the two internal phosphorus atoms of a P4-type tetraphos ligand, have been used in comparable dimers also containing oligophosphines [12]. In **1** the Pt(1)···P(2)···P(2a)···Pt(1a) torsional angle is crystallographically constraint and 180°, whereas in **2** the corresponding angle of 99.1° is considerably smaller (see Fig. 2). A major consequence for the two completely different rotation isomers is that the two central phenyl rings attached to P(2) and P(2a) are now orientated away from each other thus minimizing steric interactions in **1** and **2**.

A similar difference in the M- - -P_{int}- - -P'_{int}- - -M′ torsional angles for the *meso*- and *rac*-diastereomers of 160 and 106°, respectively, has been found in *meso*-(**10**) and *rac*-[Ni_2Cl_4(eLTTP)] (**11**), where eLTTP is ($Et_2PCH_2CH_2$(Ph)PCH_2P(Ph)$CH_2CH_2PEt_2$) [13]. Furthermore, the M- - -M′ separations are roughly paralleling the M- - -P_{int}- - -P'_{int}- - -M′ torsional angles with a lower value of the torsional angle leading to a smaller M- - -M′ distance [14]. The difference of the Ni- - -Ni′ distances in **10** and **11** of 6.272(1) and 5.417(1) Å, respectively, nicely corresponds to the difference of the Pt···Pt′ separations in **1** and **2** of 6.916(1) and 6.338(1) Å.

It has been proposed that larger than ideal M–P–CH_2 angles are indicative of sterical strain [13,1a]. The Pt(1)–P(2)–C(3) angle in **1** is 115.4°, whereas the corresponding value for **2** is only 112.3°. Together with the fact that only in **1** do the chloride and phosphorus ligands surrounding a platinum atom deviate from a plane (see above), this could indicate increased sterical strain in **1** compared with **2**.

As already mentioned, both **1** and **2** dissociate in CH_2Cl_2 solution giving cationic species with chloro bridges (compare structure A in Scheme 1). Fig. 3 shows the $^{195}Pt\{^1H\}$ NMR spectrum of **2** consisting of a doublet of doublets and clearly indicating that the two Pt(II) centers remain equivalent in solution. The corresponding spectrum of **1** is very similar and the ^1J(Pt,P) values are in agreement with the observed ^1J(Pt,PPh) and ^1J(Pt,PPh_2) parameters from the $^{31}P\{^1H\}$ spectra of **1** and **2** [1a]. The ^3J(Pt,PPh) coupling is not resolved.

Upon $NaBH_4$ reduction of *rac*-[Pt_2Cl_2(μ-Cl)P4](BF_4) the three chloride ligands of structure type A are replaced by hydride leading to structure B in *rac*-[Pt_2H_2(μ-H)P4](BF_4) (**3**). The ^1H NMR spectrum in the hydride region of **3** shows a broad quintet of triplets centered at $\delta = -0.22$ ppm. This pattern indicates fluxional behavior for **3** and averaging, which persists down to −90 °C. The quintet of relative intensity 1:8:18:8:1 is a result of the superposition of three subspectra produced by the P4Pt–Pt, P4Pt–^{195}Pt, and P4^{195}Pt–^{195}Pt isotopomers [15]. The signals are separated by $\frac{1}{2}$ ^1J(Pt,H), where ^1J(Pt,H) is 594 Hz. The binomial triplets are a consequence of the coupling to two equivalent PPh groups (see below) with ^2J(PPh,H) of 73 Hz. The coupling to the PPh_2 groups is not resolved.

The $^{31}P\{^1H\}$ NMR spectral parameters of **3** are summarized in Table 4. The $^{31}P\{^1H\}$ NMR spectrum of **3** has been simulated using the program PANIC. A

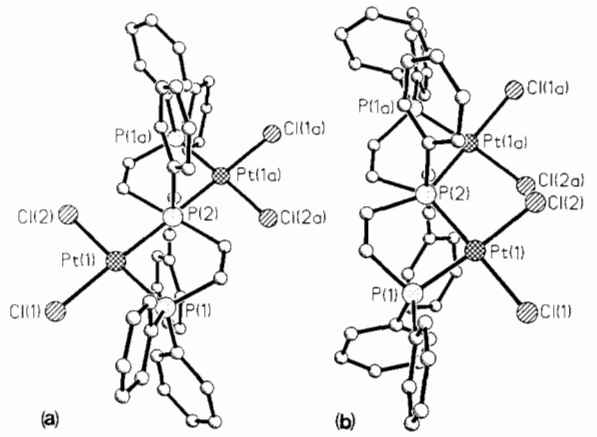

Fig. 2. Views perpendicular to the central P(2)- - -P(2a) vectors for: (a) *cis,meso*-[Pt_2Cl_4P4] (**1**) and (b) *cis,rac*-[Pt_2Cl_4P4] (**2**) (from ref. [1a]).

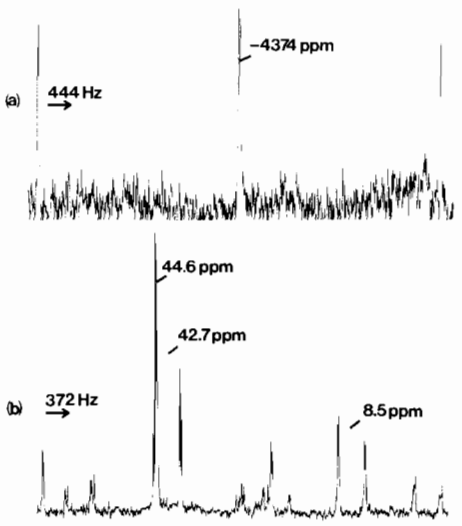

Fig. 3. (a) $^{195}Pt\{^1H\}$ NMR spectrum at 43.02 MHz and 298 K of a CH_2Cl_2 solution of *cis,rac*-[Pt_2Cl_4P4] (**2**); (b) $^{31}P\{^1H\}$ NMR spectrum at 80.96 MHz and 298 K of a CH_2Cl_2 solution of *rac*-[Pt_2Cl_2(μ-Cl)(μ-dppa)P4](BPh_4) (**8**).

Table 4
$^{31}P\{^1H\}$ NMR data for **3–9**[a]

Compound	δPPh	δPPh_2	^1J(Pt,PPh)	^1J(Pt,PPh_2)	^3J(Pt,PPh)
3	53.4	48.6	3455	4358	263[b]
4	40.7d(48)	39.7d(48)	4099	1649	
	38.7	39.1	4153	1726	56
5	41.1d(50)	40.2d(50)	4103	1652	
	39.0	39.5	4154	1682	57
6	42.0	37.7	3309	3150	
7	38.0		3200		
8[c]	42.7d(395)	44.6d(12)	2620	3446	37
9[d]	48.0d(34)	39.9d(34)	3601	3628	59
	46.2d(58)	39.8d(58)	1741	3634	

[a] J values in Hz. d = doublet, dd = doublet of doublets. J(P,P) values are given in parentheses. Spectra were run at 298 K and 80.96 MHz. The following solvents were used: CH_2Cl_2 (**3–5**, **8**, **9**), DMF (**6**), DMF/MeOH (1:1) (**7**).
[b] $^3J(Pt,PPh_2) = 114$.
[c] $\delta PPh_2(dppa) = 8.5dd(395,12)$, $^1J(Pt,PPh_2(dppa)) = 2262$.
[d] $^2J(Sn,PPh) = 1511$, $^2J(Sn,PPh_2)$ is not resolved.

full analysis of this spectrum allows establishment of, inter alia, the ^2J(Pt,Pt) value of 848 Hz [16]. The ^1H and $^{31}P\{^1H\}$ NMR parameters of **3** are in agreement with structure type B in Scheme 1, showing fast exchange between terminal and bridging hydride positions. This also accounts for the larger and only observable ^2J(PPh,H) coupling and the lower ^1J(Pt,PPh) parameter compared with ^1J(Pt,PPh_2), since in structure B the PPh groups are *trans* to the terminal hydrides [17]. However, the solid state structure seems to deviate from structure B, as no absorptions due to terminal Pt–H stretching modes could be observed in the IR spectrum of **3**. A possible explanation is a μ_2-bridging of all three hydrides leading to *rac*-$[Pt_2(\mu\text{-}H)_3P4](BF_4)$ in the solid state, since absorptions due to bridging hydrides are usually not observed [15].

A comparison with the thoroughly studied dinuclear trihydride $[Pt_2H_3(Ph_2P(CH_2)_2PPh_2)_2](BPh_4)$ (**12**) [15,18] confirms this explanation. In solution both **12** and **3** show fluxional behavior leading to very similar ^1H and $^{31}P\{^1H\}$ NMR parameters. However, in the solid state the rapid exchange of the terminal and bridging hydrides is 'frozen out' and **12** contains two μ_2-bridging hydrides in accordance with the formulation $[Pt_2H(\mu\text{-}H)_2(Ph_2P(CH_2)_2PPh_2)_2](BPh_4)$. Though containing a different phosphine ligand, a comparable deviation of the solid state structure from the solution structure could also occur in **3**.

Replacement of the central chloro bridge in *cis,rac*-$[Pt_2Cl_4P4]$ (**2**) (structure A, Scheme 1) by pyridine and simultaneous exchange of the Cl^- anion by $(BPh_4)^-$ leads to *rac*-$[Pt_2Cl_2(\mu\text{-}C_5H_5N)P4](BPh_4)_2$ (**4**). The $^{31}P\{^1H\}$ NMR spectral parameters of **4** are summarized in Table 4 and are in agreement with structure type C in Scheme 1. The formation of only one product is explained by the twofold combination of the moderately high *trans* effect of the PPh_2 groups with the low *trans* effect of the nitrogen ligand, which is possible only in the two-electron three-center binding position of pyridine shown in structure C. A preferential binding of pyridine for similar reasons has been found in comparable complexes [19,20]. The *trans* positions of the nitrogen ligand and the PPh_2 groups are clearly indicated by the smaller ^1J(Pt,PPh_2) values compared with ^1J(Pt,PPh) reflecting the stronger *trans* influence of nitrogen versus chlorine [21]. The quadrupolar effect of ^{14}N is effectively decoupled from ^{31}P due to the solution dynamic of pyridine containing complexes also observed in related compounds [19].

In **4** only the PPh group at $\delta = 38.7$ ppm shows a ^3J(Pt,PPh) coupling of 56 Hz (Table 4), which is comparable to the corresponding values in **1** and **2** (64 and 54 Hz, respectively) [1a]. In one half of **4** a $^2J(PPh_2,PPh) + {}^3J(PPh_2,PPh)$ coupling of 48 Hz occurs, which is in the *cis* range [4a]. Thus **4** shows a marked asymmetry with respect to the two halves of the molecule. An asymmetric tilting of the Pt(II) coordination and the heterocycle planes could be responsible for this effect, where this phenomenon is common for Pt(II) complexes with aromatic N-heterocycles having a phosphine ligand in a *trans* position [22].

A replacement of the central chloro bridge in **2** (structure A, Scheme 1) by the pyrazolate anion (Pz) leads to *rac*-$[Pt_2Cl_2(\mu\text{-}Pz)P4](BPh_4)$ (**5**). The $^{31}P\{^1H\}$ NMR data for **5** are summarized in Table 4. They are very similar to the corresponding values in **4**. For the reasons mentioned above the NMR parameters of **5** are in agreement with structure D (Scheme 1), where the pyrazolate anion is in a μ-η^1-bridging position. A monodentate behavior of pyrazolate groups and pyrazoles has been already observed [23]. However, as in the case of **4** μ-η^1-bridging N-heterocycles are rare [24].

A substitution of the chloro bridge in **1** or **2** by imidazolate (Im) leads to *meso*- (**6**) and *rac*-[$Pt_2Cl_2(\mu$-Im]P4](BPh$_4$) (**7**). The $^{31}P\{^1H\}$ NMR parameters of **6** and **7** (Table 4) are in agreement with structure type D in Scheme 1, where both nitrogen atoms of imidazolate are coordinated to platinum (see below). The *trans* positions of the nitrogen atoms and the PPh_2 groups are clearly indicated by the smaller $^1J(Pt,PPh_2)$ value compared with $^1J(Pt,PPh)$ in **6**. However, the quadrupolar effect of ^{14}N leads to broad signals with the *trans* PPh_2 groups being more affected in **6**, and in **7** the PPh and PPh_2 resonances coincide.

A protonation experiment with HBF_4 confirms the μ-η^2-bridging coordination of imidazolate in **6** and **7**. Besides other products it leads to a compound with $^{31}P\{^1H\}$ NMR parameters similar to **4** and **5**. They are attributed to a complex of structure D containing imidazolate in a μ-η^1-bridging position comparable to the coordination of the N-heterocycles in **4** and **5**. Obviously upon protonation of **6** or **7** only one nitrogen of imidazolate remains coordinated and the above described onset of the solution dynamic of the N-heterocycle leads to sharp $^{31}P\{^1H\}$ NMR resonances. The bridging mode of imidazolate in **6** and **7** with two coordinated nitrogen atoms is the usually observed bridging coordination for N-heterocycles containing two nitrogen atoms [6,23c].

Addition of 1,2-bis(diphenylphosphino)acetylene (dppa) to **2** (structure A, Scheme 1) and simultaneous replacement of the Cl^- anion by $(BPh_4)^-$ leads to *rac*-[$Pt_2Cl_2(\mu$-Cl)(μ-dppa)P4](BPh$_4$) (**8**). The $^{31}P\{^1H\}$ NMR spectrum of **8** is shown in Fig. 3(b) and the corresponding $^{31}P\{^1H\}$ NMR parameters are summarized in Table 4. They are in agreement with structure type E (Scheme 1), which contains dppa in an μ-η^2-binding mode. The *trans* positions of the PPh groups of P4 and the PPh_2 groups of dppa are clearly indicated by $^2J(PPh,PPh_2(dppa))$ of 395 Hz typical for the $^2J(P,P)$ *trans* range [21,25]. The smaller $^1J(Pt,PPh)$ and $^1J(Pt,PPh_2(dppa))$ values compared with $^1J(Pt,PPh_2)$ are also in accordance with this coordination. The $^3J(Pt,PPh)$ coupling of 37 Hz shows the presence of the chloro bridge.

8 is a rare example of two five-coordinate Pt(II) centers triply bridged by two different phosphorus ligands, P4 and dppa, respectively, and by chloride. The coordination of dppa via the two phosphorus centers, with the acetylenic bond coordinatively inactive is common [26]. Furthermore, the bridging position of dppa in **8** is clearly favored by its incapability to chelate a metal center [7a,27]. The $Pt_2(\mu$-Cl)P_4 core of **8** (compare Scheme 1) resembles the well-known A-frame molecules [8a].

Oxidative addition of $SnCl_2$ to *cis,meso*-[$Pt_2Cl_2(\mu$-Cl)P4](BPh$_4$) leads to *meso*-[$Pt_2Cl(\mu$-Cl)($SnCl_3$)P4]-(BPh$_4$) (**9**). The $^{31}P\{^1H\}$ NMR parameters of **9** (Table 4) are in agreement with structure F in Scheme 1. The four distinct $^{31}P\{^1H\}$ resonances clearly indicate the asymmetry of **9**. Both the reduction of the $^1J(Pt,PPh)$ value to 1741 Hz and the occurrence of a $^2J(Sn,PPh)$ coupling of 1511 Hz are in line with the *trans* position of the $(SnCl_3)^-$ ligand to one PPh group [28]. The presence of the chloro bridge is shown by the $^3J(Pt,PPh)$ coupling (59 Hz) of the PPh group at $\delta = 48.0$ ppm. Though the possibility of a $SnCl_2$-bridged species is precedented [8] only a terminal Pt–Cl bond is inserted by $SnCl_2$ in **9**.

4. Discussion

The most striking result is that with the exception of the imidazolate containing complexes the compounds B–F (Scheme 1) could only be obtained in one diastereomeric form, respectively. Attempts to prepare the other diastereomers yield mixtures of products, where monomeric species are also involved. The X-ray structures of *cis,meso*- (**1**) and *cis,rac*-[Pt_2Cl_4P4] (**2**) show that in both cases the phenyl rings belonging to the PPh groups are rotated away from each other thus minimizing intramolecular contact approaches. This leads to different orientations of the two halves of **1** and to almost the same orientation in **2** (see Fig. 2). Since it seems likely, that the same steric effect also occurs in solution the formation of bridges between the P4 coordination units is favored in **2**. Also in the cases of *meso*- (**10**) and *rac*-[Ni_2Cl_4(eLTTP)] (**11**) the solution structures closely resemble the X-ray structures [13]. However, van der Waals energy calculations have shown that for M_2(eHTP) bimetallic systems, where M is Ni, Pd or Pt and eHTP is $(Et_2PCH_2CH_2)_2PCH_2P(CH_2CH_2PEt_2)_2$, a variety of low-energy rotational conformations are accessible [14]. If these conformations also occur in **1** and **2**, the possibility of the incorporation of a bridging ligand will strongly depend on its very steric and electronic nature. This could explain the fact that chloro and imidazolate bridges are also possible for the *meso*-diastereomers in **1** and **6**. Further work on this is in progress.

5. Supplementary material

Tables of thermal parameters (1 page), bond lengths and bond angles (2 pages), torsion angles, H atom coordinates and non-bonded distances (3 pages), and structure factors (17 pages) are available from the author on request.

Acknowledgement

We thank the Fonds zur Förderung der wissenschaftlichen Forschung, Austria, for financial support.

References

[1] (a) H. Goller and P. Brüggeller, *Inorg. Chim. Acta, 197* (1992) 75; (b) J.-D. Chen, F.A. Cotton and B. Hong, *Inorg. Chem., 32* (1993) 2343.
[2] E.C. Constable, S.M. Elder, J. Healy, M.D. Ward and D.A. Tocher, *J. Am. Chem. Soc., 112* (1990) 4590.
[3] J.W. Ellis, K.N. Harrison, P.A.T. Hoye, A.G. Orpen, P.G. Pringle and M.B. Smith, *Inorg. Chem., 31* (1992) 3026.
[4] (a) P. Brüggeller, *Inorg. Chem., 29* (1990) 1742; (b) P. Brüggeller, *Acta Crystallogr., Sect. C, 48* (1992) 445.
[5] (a) M.M. Muir, O. Cox, L.A. Rivera, M.E. Cadiz and E. Medina, *Inorg. Chim. Acta, 191* (1992) 131; (b) J.A. Broomhead, L.M. Rendina and M. Sterns, *Inorg. Chem., 31* (1992) 1880.
[6] (a) J.-P. Costes, F. Dahan and J.-P. Laurent, *Inorg. Chem., 30* (1991) 1887; (b) J.C. Bayon, P. Esteban, G. Net, P.G. Rasmussen, K.N. Baker, C.W. Hahn and M.M. Gumz, *Inorg. Chem., 30* (1991) 2572; (c) M.I. Bruce, M.G. Humphrey, O.B. Shawkataly, M.R. Snow and E.R.T. Tiekink, *J. Organomet. Chem., 336* (1987) 199; (d) Z.W. Mao, K.B. Yu, D. Chen, S.Y. Han, Y.X. Sui and W.X. Tang, *Inorg. Chem., 32* (1993) 3104.
[7] (a) E. Sappa, *J. Organomet. Chem., 352* (1988) 327; (b) M.I. Bruce, M.J. Liddell and E.R.T. Tiekink, *J. Organomet. Chem., 391* (1990) 81; (c) L.J. Farrugia, N. MacDonald and R.D. Peacock, *J. Chem. Soc., Chem. Commun.,* (1991) 163.
[8] (a) A.R. Sanger, *Inorg. Chim. Acta, 191* (1992) 81; (b) I.R. Herbert, P.S. Pregosin and H. Ruegger, *Inorg. Chim. Acta, 112* (1986) 29.
[9] A.C.T. North, D.C. Phillips and F.S. Mathews, *Acta Crystallogr., Sect. A, 24* (1968) 351.
[10] G.M. Sheldrick, SHELXS86, in G.M. Sheldrick, C. Krüger and R. Goddard (eds.), *Crystallograhic Computing 3*, Oxford University Press, London, 1985, p. 175.
[11] J.M. Brown and L.R. Canning, *J. Organomet. Chem., 267* (1984) 179.
[12] S.A. Laneman and G.G. Stanley, *Inorg. Chem., 26* (1987) 1177.
[13] S.A. Laneman, F.R. Fronczek and G.G. Stanley, *Inorg. Chem., 28* (1989) 1872.
[14] S.E. Saum, S.A. Laneman and G.G. Stanley, *Inorg. Chem., 29* (1990) 5065.
[15] C.B. Knobler, H.D. Kaesz, G. Minghetti, A.L. Bandini, G. Banditelli and F. Bonati, *Inorg. Chem., 22* (1983) 2324.
[16] T.H. Tulip, T. Yamagata, T. Yoshida, R.D. Wilson, J.A. Ibers and S. Otsuka, *Inorg. Chem., 18* (1979) 2239.
[17] G. Minghetti, A.L. Bandini, G. Banditelli, F. Bonati, R. Szostak, C.E. Strouse, C.B. Knobler and H.D. Kaesz, *Inorg. Chem., 22* (1983) 2332.
[18] (a) M.Y. Chiang, R. Bau, G. Minghetti, A.L. Bandini, G. Banditelli and T.F. Koetzle, *Inorg. Chem., 23* (1984) 122; (b) S. Aime, R. Gobetto, A.L. Bandini, G. Banditelli and G. Minghetti, *Inorg. Chem., 30* (1991) 316.
[19] W. Kaufmann, L.M. Venanzi and A. Albinati, *Inorg. Chem., 27* (1988) 1178.
[20] N.W. Alcock, P.G. Pringle, P. Bergamini, S. Sostero and O. Traverso, *J. Chem. Soc., Dalton Trans.,* (1990) 1553.
[21] K.D. Tau and D.W. Meek, *Inorg. Chem., 18* (1979) 3574.
[22] A. Albinati, F. Isaia, W. Kaufmann, C. Sorato and L.M. Venanzi, *Inorg. Chem., 28* (1989) 1112.
[23] (a) G.A. Ardizzoia, E.M. Beccalli, G. La Monica, N. Masciocchi and M. Moret, *Inorg. Chem., 31* (1992) 2706; (b) M.A. Cinellu, S. Stoccoro, G. Minghetti, A.L. Bandini, G. Banditelli and B. Bovio, *J. Organomet. Chem., 372* (1989) 311; (c) G. Banditelli, A.L. Bandini, F. Bonati and G. Minghetti, *Inorg. Chim. Acta, 60* (1982) 93.
[24] (a) C. Piguet, G. Bernardinelli and A.F. Williams, *Inorg. Chem., 28* (1989) 2920; (b) C. Lorenzini, C. Pelizzi, G. Pelizzi and G. Predieri, *J. Chem. Soc., Dalton Trans.,* (1983) 2155; (c) C. Mealli, C.S. Arcus, J.L. Wilkinson, T.J. Marks and J.A. Ibers, *J. Am. Chem. Soc., 98* (1976) 711.
[25] P. Brüggeller, *Inorg. Chim. Acta, 155* (1989) 45.
[26] O. Orama, *J. Organomet. Chem., 314* (1986) 273.
[27] H.C. Bechthold and D. Rehder, *J. Organomet. Chem., 172* (1979) 331.
[28] (a) K.H.A. Ostoja Starzewski, P.S. Pregosin and H. Rüegger, *Helv. Chim. Acta, 65* (1982) 785; (b) P. Brüggeller, *Z. Naturforsch., Teil B, 41* (1986) 1561.